

## Article

# Crystal Structure of Hydrotalcite Group Mineral—Desautelsite, $\text{Mg}_6\text{Mn}^{\text{III}}_2(\text{OH})_{16}(\text{CO}_3)\cdot 4\text{H}_2\text{O}$ , and Relationship between Cation Size and In-Plane Unit Cell Parameter

Elena S. Zhitova <sup>1,\*</sup> , Rezeda M. Sheveleva <sup>1,2</sup>, Anatoly V. Kasatkin <sup>3</sup> , Andrey A. Zolotarev <sup>1,4</sup> , Vladimir N. Bocharov <sup>5</sup> , Anastasia N. Kupchinenko <sup>1</sup> and Dmitry I. Belakovsky <sup>3</sup>

<sup>1</sup> Institute of Volcanology and Seismology, Far East Branch of Russian Academy of Sciences, Piipa Blvd. 9, 683006 Petropavlovsk-Kamchatsky, Russia; rezeda\_marsova@inbox.ru (R.M.S.); aazolotarev@gmail.com (A.A.Z.)

<sup>2</sup> Research Part of the Institute of Geosciences, Saint-Petersburg State University, 199034 Saint-Petersburg, Russia

<sup>3</sup> Fersman Mineralogical Museum, Russian Academy of Science, Leninskiy Prospekt 18-2, 119071 Moscow, Russia; kasatkin@inbox.ru (A.V.K.)

<sup>4</sup> Crystallography Department, Saint-Petersburg State University, Dekabristov 16, 199155 Saint-Petersburg, Russia

<sup>5</sup> Geomodel Resource Centre, Saint-Petersburg State University, 198504 Saint-Petersburg, Russia

\* Correspondence: zhitova\_es@mail.ru

**Abstract:** The crystal structure of a naturally occurring layered double hydroxide mineral—desautelsite from San Benito County, California, USA—was refined using single-crystal X-ray diffraction data in the space group  $R\bar{3}m$ ,  $a = 3.1238(2) \text{ \AA}$ ,  $c = 23.528(3) \text{ \AA}$ ,  $V = 198.83(4) \text{ \AA}^3$ , and  $Z = 3/8$ . The Mg and Mn cations are disordered occurring in one  $M$  site with occupancy  $\text{Mg}_{0.77}\text{Mn}_{0.23}$ . According to the electron microprobe analysis supported by Raman spectroscopy, the empirical formula is  $\text{Mg}_{6.20}(\text{Mn}^{\text{III}}_{1.78}\text{Al}_{0.01}\text{Fe}^{\text{III}}_{0.01})_{\Sigma 1.80}(\text{OH})_{16}(\text{CO}_3)_{0.90}\cdot 5.35\text{H}_2\text{O}$  that shows higher content of interlayer ( $\text{H}_2\text{O}$ ) molecules in comparison to the ideal formula that also agrees with the structure refinement. The Raman spectroscopy of two samples indicated O–H vibrations ( $3650/3640 \text{ cm}^{-1}$ ,  $\sim 3500 \text{ sh cm}^{-1}$ ), symmetric C–O ( $1055/1057 \text{ cm}^{-1}$ ), Mg–O–Mg ( $533/533 \text{ cm}^{-1}$ ) and Mn–O–Mn ( $439/438 \text{ cm}^{-1}$ ) stretching vibrations and lattice vibrations ( $284/287 \text{ cm}^{-1}$ ). Summing up our data and that of the current literature, we show a correlation ( $R^2 = 0.91$ ) between the averaged effective ionic radius ( $x$ ) and  $a$  unit cell parameter ( $y$ ) of hydrotalcite group minerals,  $y = 1.9871x + 1.4455$ . Desautelsite follows this correlation, being the species with one of the largest  $a$  unit cell parameters among the group. The correlation can be applied for control of cation intercalation during synthesis.

**Keywords:** desautelsite; layered double hydroxide (LDH); structure; mineral; Raman; chemical composition; cation; radii; radius; size; correlation



**Citation:** Zhitova, E.S.; Sheveleva, R.M.; Kasatkin, A.V.; Zolotarev, A.A.; Bocharov, V.N.; Kupchinenko, A.N.; Belakovsky, D.I. Crystal Structure of Hydrotalcite Group Mineral—Desautelsite,  $\text{Mg}_6\text{Mn}^{\text{III}}_2(\text{OH})_{16}(\text{CO}_3)\cdot 4\text{H}_2\text{O}$ , and Relationship between Cation Size and In-Plane Unit Cell Parameter. *Symmetry* **2023**, *15*, 1029. <https://doi.org/10.3390/sym15051029>

Academic Editor: György Keglevich

Received: 3 April 2023

Revised: 25 April 2023

Accepted: 30 April 2023

Published: 5 May 2023



**Copyright:** © 2023 by the authors. Licensee MDPI, Basel, Switzerland. This article is an open access article distributed under the terms and conditions of the Creative Commons Attribution (CC BY) license (<https://creativecommons.org/licenses/by/4.0/>).

## 1. Introduction

Layered double hydroxides (LDHs) represent a class of anion-exchange materials with various catalytic, pharmaceutical, electrochemical and other applications [1–7]. Their crystal structures are built of positively charged metal-hydroxide layers  $[\text{M}^{\text{II}}_{1-x}\text{M}^{\text{III}}_x(\text{OH})_2]^{x+}$  (in the case of di- and trivalent LDHs) and negatively charged interlayers  $[(\text{A}^{n-})_{x/n}\cdot y\text{H}_2\text{O}]^{x-}$ , where  $\text{M}^{\text{II}}$  and  $\text{M}^{\text{III}}$  are di- and trivalent cations,  $A$  is an anion of  $n$  charge,  $x$  is variable with  $x = 0.33$  and  $x = 0.25$  being the most widespread values ( $x = 0.33$  is considered the upper limit; the lower limit is not determined but likely 0.143 (by appearance of questionable mineral brugnatellite) or above), and  $y$  is variable. Among synthetic artificially obtained phases, there are hundreds of LDHs of various compositions [8], which are obtained by combining various divalent and trivalent cations and anions, and anions can also represent inorganic species or organic molecules [9]. The number of minerals, i.e., layered

double hydroxides formed under completely natural conditions, is much more limited and amounts to about 50 phases (including very newly approved, but not published minerals) forming the hydrotalcite supergroup [10]. These minerals can be considered stable long-lived prototype phases, which often occur in crystals, and their growth is not limited by time. Such crystals can be subjected to a number of methods of investigation (including single-crystal X-ray diffraction), which are unsuitable for synthetic fine-grained phases.

Desautelsite,  $\text{Mg}_6\text{Mn}^{\text{III}}_2(\text{OH})_{16}(\text{CO}_3)\cdot 4\text{H}_2\text{O}$ , is described as a pyroaurite-related mineral from the Cedar Hill quarry, Lancaster county, Pennsylvania (type locality) and two localities in San Benito County, CA, USA [11] where it forms at the last stage of mineral formation in fractured serpentinites. The mineral occurs as tabular hexagonal crystals of a rather specific, for hydrotalcite-supergroup minerals, bright orange colour (Figure 1). Desautelsite has also been described in detail from Konomori, Kochi City, Japan where a desautelsite-bearing fissure is found in fractured serpentinites of ultrabasic rocks, and the mineral is supposedly found in five other places in Japan [12]. Desautelsite belongs to the hydrotalcite group that combines species with  $M^{\text{II}}:M^{\text{III}}\sim 3:1$  and  $(\text{CO}_3)^{2-}$ ,  $\text{Cl}^-$  and  $(\text{OH})^-$  anions [10]. Desautelsite is a  $\text{Mn}^{\text{III}}$ -analogue of hydrotalcite, pyroaurite and stichtite.



**Figure 1.** Orange desautelsite and white artinite on serpentinite rock. Sample 29D. Photo size is  $6 \times 4 \times 3$  cm.

The crystal structure of desautelsite has been previously determined based on the material from San Benito County, CA, USA [11] in  $R3m$  or  $R\bar{3}m$  space group, with  $a = 3.114(1)$ ,  $c = 23.39(2)$  Å,  $V = 196.4$  Å<sup>3</sup>, and  $Z = 3/8$ . The crystal structure has been described as consisting of octahedral sheets with Mg and Mn being disordered (found in one site) and statistically disordered interlayer species of  $(\text{CO}_3)^{2-}$  and  $(\text{H}_2\text{O})^0$  sandwiched between them. However, authors noted [11] that due to the expected Jahn-Teller distortion of  $\text{Mn}^{\text{III}}(\text{OH})_6$  octahedra coupled with the difference in the ionic charge and radius between  $\text{Mg}^{\text{II}}$  and  $\text{Mn}^{\text{III}}$ , the ordering of Mg and Mn cations could be expected, but this was not registered and can be short-range in the nature. Despite the fact that desautelsite is a rare example, when the crystal structure is solved and refined based on data obtained by

a reliable and accurate single-crystal X-ray diffraction method, the speculations on the absence or presence of long-range ordering of Mg and Mn, and hence on the symmetry of the mineral, remained [13,14]. In the 44 years that have passed since the structural study of desautelsite, analytical equipment has made great strides forward, which, for example, made it possible to determine the crystal structures of LDH with cationic [15–20] and/or anionic [21–24] ordering using single-crystal X-ray diffraction data. Recently, using the example of hydrotalcite,  $\text{Mg}_6\text{Al}_2(\text{OH})_{16}(\text{CO}_3)\cdot 4\text{H}_2\text{O}$ , it has been shown that there is no long-range order for Mg and Al in octahedral sheets [25]. Despite the fact that hydrotalcite is an important mineral as it is the archetype of the supergroup [10], Mg and Al cations have a similar scattering power which theoretically could complicate the identification of potential superstructures. The very specific thing about desautelsite is its chemistry since this is the only hydrotalcite-supergroup mineral with  $\text{Mn}^{\text{III}}$  and it is still not entirely clear whether this peculiarity of the chemical composition may affect its crystal structure. Thus,  $\text{Mg}^{\text{II}}$  and  $\text{Mn}^{\text{III}}$  cations differ much more in terms of scattering power, size and specificity owing to the Jahn-Teller distortion of Mn-centred octahedra. Accordingly, desautelsite is an interesting object among LDHs for structural determination and refinement. In this study we provide the re-investigation of desautelsite from San Benito County, CA, USA by electron microprobe analysis, Raman spectroscopy, and powder and single-crystal X-ray diffraction that is required for modern mineral characterization and identification in order to reveal its internal atomic structure. Then, using the data obtained in the work and previously published data for LDH minerals, the relationship between the effective ionic radius (crystal radius by [26]) and the in-plane  $a$  unit cell parameter is shown.

## 2. Materials and Methods

### 2.1. Materials

In this study, we investigated two desautelsite samples found in nature: (1) from the systematic collection of the Fersman Mineralogical Museum of the Russian Academy of Science (Moscow) under catalog number 80137 and (2) from the personal collection of AVK (third author) denoted as 29D. Both specimens originate from the Artinite Pit, Picacho Peak, San Benito County, CA, USA (Latitude and Longitude (WGS84):  $36^\circ$  North,  $120^\circ$  West) [27]. Specimen 80137 was obtained by exchange with Excalibur Mineral Co, in 1979. Desautelsite is represented by orange-brown patches consisting of aggregates of thin plates on serpentine associating with white sprays of artinite. The specimen looks like the typical material from Artinite Pit, Picacho Peak, San Benito County, CA, USA and most likely was collected there, while the locality on the label is given as «near Gem Mine, San Benito County, CA, USA». The Artinite Pit is about 5 miles from the gem mine made famous by classic specimens of benitoite and neptunite.

Both samples occur as hexagonal platy crystals forming rosette-like aggregates (Figure 2). In sample 29D, desautelsite occurs as an orange crust composed of hexagonal lamellar crystals up to 0.05 mm on serpentinite rock in association with white radiating sprays of artinite (Figure 1). The matrix consists of dominant lizardite with calcite, siderite, andradite and tiny awaruite inclusions (Figure 3).

### 2.2. Methods

#### 2.2.1. Chemical Analysis

Sample 80137 was placed on carbon tape (Figure 2), carbon-coated and subjected to investigation by a scanning electron microscope Hitachi S-3400N equipped with an Oxford X-Max 20 energy-dispersive spectrometer (Geomodel Center of St. Petersburg State University) operating in the energy dispersive spectroscopy (EDS) mode at an accelerating voltage of 20 kV, a beam current of 0.5 nA; the electron beam diameter was 5  $\mu\text{m}$ . The standards used for quantification were MgO (Mg) and Mn (Mn).

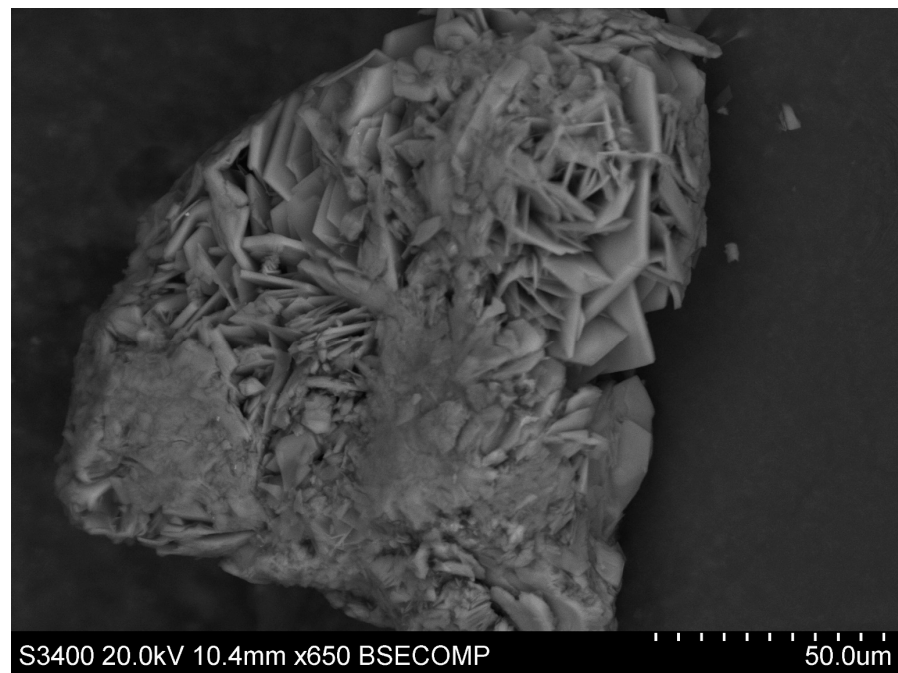


**Figure 2.** Back-scattered electron image of desautelsite forming hexagonal plates. Sample 80137.

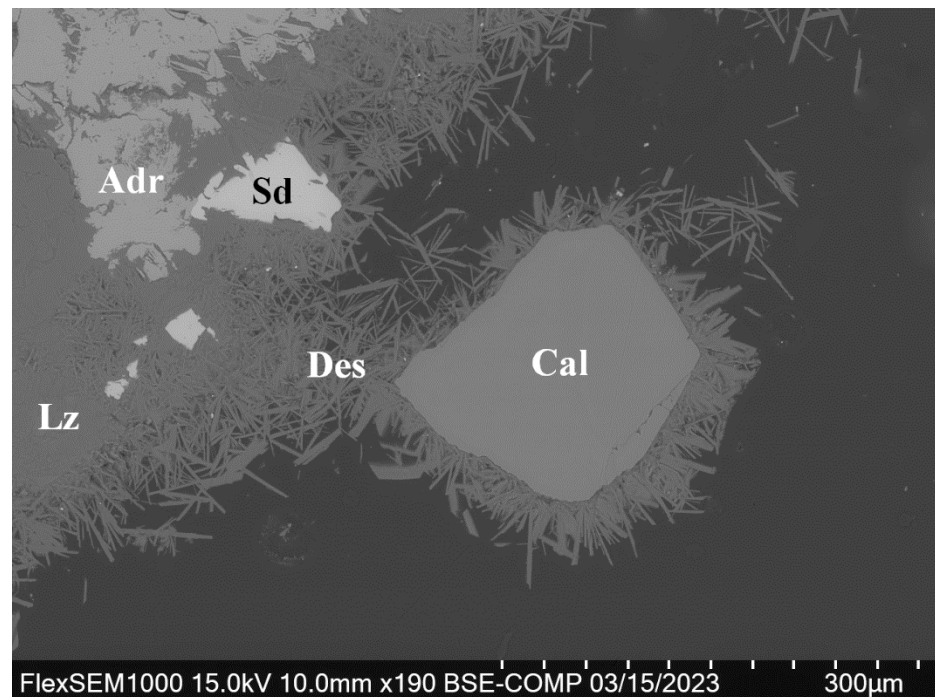


**Figure 3.** Cross-sections of lamellar desautelsite (Des) crystals overgrowing calcite (Cal) and lizardite (Lz) with andradite (Adr) and siderite (Sd). Scanning-electron microscopy image was obtained in back-scattered electrons. Mineral symbols are by [28]. Sample 29D.

Sample 29D was placed in epoxy resin, polished (Figure 3), carbon-coated and studied with a Hitachi FlexSEM 1000 scanning electron microscope equipped with EDS Xplore Contact 30 detector and Oxford AZtecLive STD system of analysis. Analytical conditions were accelerating voltage 15 kV, beam current 5 nA and beam size 2 µm. The standards are given in Table 1.

**Table 1.** Chemical composition of desautelsite, sample 29D.

Constituent	wt. %	Range	Stand. Dev.	Standards
MgO	37.23	35.47–38.60	1.08	Mg <sub>2</sub> SiO <sub>4</sub>
Al <sub>2</sub> O <sub>3</sub>	0.04	0.02–0.18	0.06	Kyanite
Mn <sub>2</sub> O <sub>3</sub>	20.90	20.47–21.27	0.32	Mn <sub>2</sub> SiO <sub>4</sub>
Fe <sub>2</sub> O <sub>3</sub>	0.09	0.02–0.18	0.05	FeS <sub>2</sub>
CO <sub>2</sub> <sup>1</sup>	5.90			
H <sub>2</sub> O <sup>2</sup>	35.84			
<b>Total</b>	<b>100.00</b>			

<sup>1</sup> Calculated by charge balance; <sup>2</sup> calculated from deficiency of analytical total.

### 2.2.2. Raman Spectroscopy

The Raman spectrum of desautelsite was obtained with a Horiba Jobin-Yvon LabRam HR800 spectrometer, equipped with a solid-state laser ( $\lambda = 532$  nm) at 50 mW output power and  $\sim 6$  mW power at the sample surface for an area of  $2 \mu\text{m} \times 2 \mu\text{m}$ . The spectrum was recorded at room temperature from randomly oriented desautelsite rosette-like aggregates placed on a glass slide and was further processed using LabSpec (Horiba) and Origin (Origin lab corp, Northhampton, MA, USA) software.

### 2.2.3. Powder X-ray Diffraction

Powder X-ray diffraction (XRD) data were collected by means of a Rigaku R-Axis Rapid II single-crystal diffractometer using Debye-Scherrer geometry (source: CoK $\alpha$ ,  $\lambda = 1.79026$  Å, voltage = 40 kV and current = 15 mA,  $d = 127.4$  mm). The diffractometer is equipped with a rotating anode, microfocus optics and a cylindrical image plate detector.

### 2.2.4. Single-Crystal X-ray Diffraction

Single-crystal X-ray diffraction analysis was carried out for desautelsite sample 29D using a four-circle diffractometer Rigaku XtaLAB Synergy-S (Oxford Diffraction, Japan) operated with a monochromated MoK $\alpha$  radiation (source: MoK $\alpha$ ,  $\lambda = 0.71073$  Å) at 50 kV and 1.0 mA and equipped with a CCD HyPix-6000HE detector. The scan width was  $1.0^\circ$ , exposition was 140 s (long exposure is characteristic of LDHs because they are normally thin, relatively weakly diffracting samples). The CrysAlisPro [29] software package was used to process the data; an empirical absorption correction was calculated based on spherical harmonics implemented in the SCALES ABSPACK algorithm.

## 3. Results

### 3.1. Chemical Composition

Ten chemical analyses were obtained for sample 80137 from an unpolished surface. Only Mg and Mn cations were found (with no detected impurities). The anion is represented by a carbonate group, and only traces of Cl registered. These results allowed the calculation of Mg:Mn proportion as  $\sim 6.2:1.8$ .

More detailed chemical data were obtained for sample 29D (that according to powder X-ray diffraction was pure of intimately associated phases, see Section 3.3) which was polished. Desautelsite was stable in a vacuum; no signs of dehydration or cracking were detected under the beam. All analyses of measured components (metal oxides) were confined to 58–59 wt.%. The results of the electron microprobe analysis for sample 29D are given in Table 1. The mineral is homogeneous in element distribution (Figure 3). Data from 11 chemical analyses of the desautelsite (sample 29D) were averaged to calculate the chemical formula of the sample. The empirical formula calculated on the basis of the sum of all metal cations = 8 *apfu* (atom per formula unit) and OH = 16 *apfu* is Mg<sub>6.20</sub>(Mn<sup>III</sup><sub>1.78</sub>Al<sub>0.01</sub>Fe<sup>III</sup><sub>0.01</sub>)<sub>Σ1.80</sub>(OH)<sub>16</sub>(CO<sub>3</sub>)<sub>0.90</sub>·5.35H<sub>2</sub>O.

This study shows that both samples are identical in chemical composition even including the Mg:Mn ratio.

### 3.2. Raman Spectroscopy

The Raman spectra of desautelsite are given in Figure 4, and the band assignment and its comparison to the literature sources are given in Table 2. In general, the Raman spectra of desautelsite are similar to the spectra measured previously for that mineral and also for stichtite and pyroaurite (Table 2). The spectra comprise bands assigned to the following vibrations: O–H stretching, antisymmetric and symmetric vibrations of C–O in CO<sub>3</sub> group, Mg–O–Mg and Mn–O–Mn vibrations and those produced by the lattice. The data also allow the conclusion that the interlayer anion is represented by a CO<sub>3</sub> group, while other functional anion groups are absent.

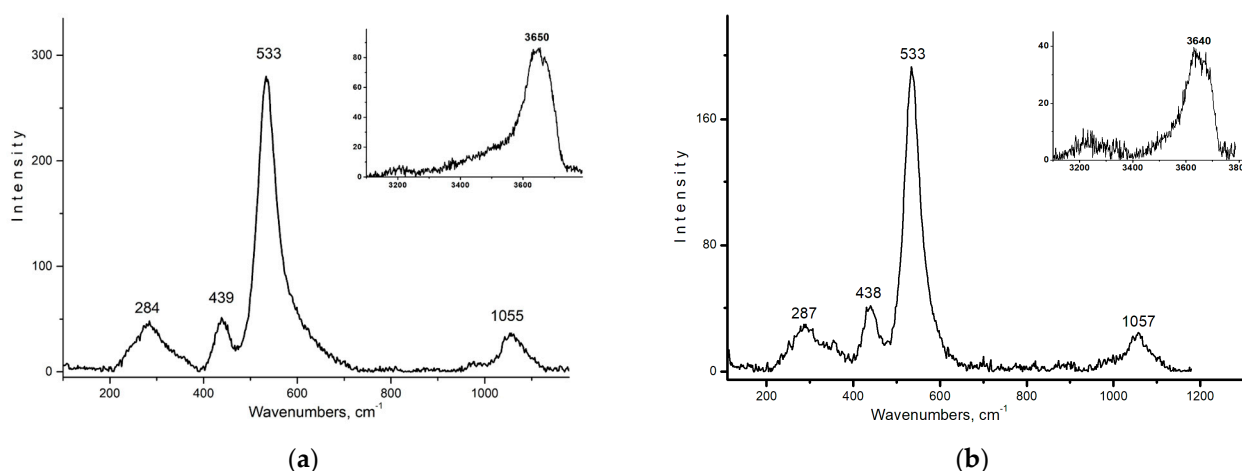


Figure 4. Raman spectra of desautelsite, sample 80137 (a) and sample 29D (b).

Table 2. Results of Raman spectroscopic analysis of desautelsite and their comparison to the literature data.

Desautelsite		Pyroaurite	Stichtite	Assignment
80137	29D	[30]	[31]	
3650	3640	3646, 3608	3600–3500	O–H stretching of OH groups
~3500 sh	~3500 sh	3509, 3409, 3325	~3300 sh	O–H stretching of H <sub>2</sub> O molecules
-	-	1393, 1349, 1342	1346	Antisymmetric stretching vibrations of CO <sub>3</sub> group
1055	1057	1086, 1062, 1055	1058	Symmetric stretching vibrations of CO <sub>3</sub> group
533	533	535	527	Mg–O–Mg [33]
439	438	455, 436, 422	-	Mn–O–Mn (desautelsite) Cr–O–Cr (stichtite)
-	-	313	-	Lattice vibrations
284	287	281	284	

### 3.3. Powder X-ray Diffraction

The data were integrated using the software package Osc2Tab/SQRay [34]. In Figure 5 we provide the powder X-ray diffraction patterns of both desautelsite samples. This study has shown that the selected fragment from sample 29D is represented solely by desautelsite, whereas the fragment from sample 80137 is found in intimate association with lizardite, Mg<sub>3</sub>(Si<sub>2</sub>O<sub>5</sub>)(OH)<sub>4</sub>, and dashkovaite, Mg(HCOO)<sub>2</sub>·2H<sub>2</sub>O. The obtained interplanar distances *d* (Å) and *hkl* indices of studied samples and comparison of these values to the type specimen [11] are given in Table 3. Both desautelsite samples crystallize as 3R polytypes, the unit-cell parameters based on reflections position for samples 29D/80137

are  $a = 3.122/3.119 \text{ \AA}$ , and  $c = 23.46/23.49 \text{ \AA}$ , respectively. Both desautelsite samples studied in this work have very similar unit-cell parameters that are somewhat different for type material (estimated by the powder X-ray diffraction data given in Table 3) that have  $a = 3.114(1) \text{ \AA}$ , and  $c = 23.39(2) \text{ \AA}$ .

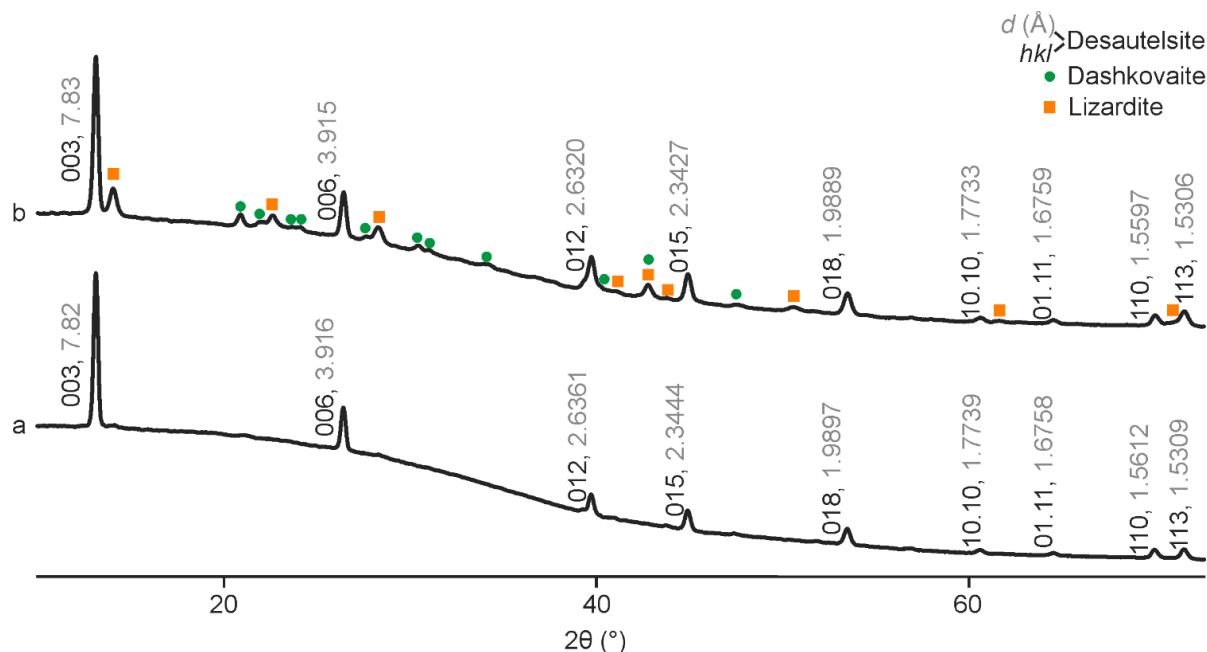


**Figure 5.** Powder X-ray diffraction pattern of desautelsite: (a) sample 29D and (b) sample 80137, where desautelsite is found in close association with lizardite,  $\text{Mg}_3(\text{Si}_2\text{O}_5)(\text{OH})_4$ , and dashkovaite,  $\text{Mg}(\text{HCOO})_2 \cdot 2\text{H}_2\text{O}$ .

**Table 3.** Powder X-ray diffraction data for two desautelsite samples compared with holotype data.

Sample 29D		Sample 80137 <sup>1</sup>		Literature Data [11]		<i>h</i>	<i>k</i>	<i>l</i>
$d_{\text{meas}}$ (Å)	$I_{\text{meas}}$ (%)	$d_{\text{meas}}$ (Å)	$I_{\text{meas}}$ (%)	$d_{\text{meas}}$ (Å)	$I_{\text{meas}}$ (%)			
7.82	100	7.83	100	7.76	100	0	0	3
3.916	27	3.915	29	3.88	60	0	0	6
2.6361	13	2.6320	21	2.622	50	0	1	2
2.3444	13	2.3427	18	2.332	60	0	1	5
1.9897	10	1.9889	14	1.981	60	0	1	8
1.7739	2	1.7733	3	1.768	20	1	0	10
1.6758	2	1.6759	2	1.670	20	0	1	11
1.5612	6	1.5597	8	1.557	20	1	1	0
1.5309	7	1.5306	10	1.527	30	1	1	3
1.5039	1	1.5022	2	1.498	30	1	0	13

<sup>1</sup> Only desautelsite reflections are presented, while dashkovaite and lizardite reflections (see Figure 5) are omitted; the full data set is provided in Table S1.

### 3.4. Crystal Structure Solution and Refinement

The single-crystal X-ray diffraction data obtained for desautelsite were indexed in the rhombohedral unit cell, space group  $R\bar{3}m$  (Table 4). The crystal structure was solved and refined to  $R_1 = 0.038$  based on 116 unique observed reflections with  $I > 2\sigma(I)$ . Atom coordinates, site occupancies and isotropic displacement parameters are given in Table 5. Selected bond lengths and angles are listed in Table 6. The crystallographic information file (cif) has been deposited via the joint Cambridge Crystal Data Centre CCDC/FIZ Karlsruhe deposition service; the deposition number is 2251692.

**Table 4.** Crystal data, data collection, and structure refinement details for desautelsite.

Crystal Chemical Data	
Crystal system	Trigonal
Space group	$R\bar{3}m$
$a$ (Å)	3.1238(2)
$c$ (Å)	23.528(3)
$V$ (Å <sup>3</sup> )	198.83(4)
$Z$	0.375
Calculated density (g/cm <sup>3</sup> )	2.111
Absorption coefficient (mm <sup>-1</sup> )	1.367
Crystal from	Hexagonal plate
Crystal size (µm)	30 × 30 × 10
Data collection	
Diffractometer	Rigaku XtaLAB Synergy-S
Temperature (K)	293
Radiation, wavelength (Å)	MoK $\alpha$ , 0.71073
Range of data collection, $\theta$ (°)	5.199–32.598
$h, k, l$ ranges	−4→4, −4→4, −33→33
Total reflection collected	1048
Unique reflections (Rint)	121 (0.0386)
Number of unique reflections $F > 2\sigma(F)$	116
Data completeness (%)	98.5
Structure refinement	
Refinement method	Full-matrix least-squares on $F^2$
Weighting coefficients a, b	0.055400, 0.373000
Data/restrain/parameters	121/2/13
$R_1$ [ $F > 2\sigma(F)$ ], $wR_2$ [ $F > 2\sigma(F)$ ]	0.0386, 0.1063
$R_1$ all, $wR_2$ all	0.0395, 0.1067
Goodness-of-fit on $F^2$	1.276
Largest diff. peak and hole (eÅ <sup>-3</sup> )	0.78, −0.23

**Table 5.** Atom coordinates, equivalent isotropic displacement parameters (Å<sup>2</sup>), site occupancies and assigned site populations for desautelsite.

Atom	$x$	$y$	$z$	$U_{eq}$	s.o.f.	Assigned Site Populations
<b>Octahedral sheet</b>						
M (Mg)	1	0	0	0.0158(5)	0.772 *	Mg <sub>0.77</sub> Mn <sub>0.23</sub> (OH) <sub>2</sub>
M (Mn)	1	0	0	0.0158(5)	0.224 *	
O1	1.3333	1/3	0.04335(11)	0.0197(6)	1 *	
H1	1.3333	1/3	0.0806(13)	0.030	1 *	
<b>Interlayer gallery</b>						
O2	1.222(2)	−0.222(2)	0.1664(17)	0.078(7)	0.186(8)	(CO <sub>3</sub> ) <sub>0.88</sub> (H <sub>2</sub> O) <sub>5</sub> **
C1	1	0	0.163(3)	0.030(15)	0.0545 *	

\* Fixed during refinement; \*\* the electron per formula unit (*epfu*) for O<sub>2</sub> site is recalculated as (H<sub>2</sub>O)<sup>0</sup>, the deviation in the calculation of (H<sub>2</sub>O)<sup>0</sup> content by structure refinement is quite high and we believe that in fact the (H<sub>2</sub>O)<sup>0</sup> content is close to the data of the electron microprobe analysis, i.e., ~5.3 *apfu*.

Positions of metal and oxygen of the metal-hydroxide layer were determined by direct methods and refined anisotropically (Table S2). The interlayer species (O and C) and hydrogen atoms were located from the inspection of difference-Fourier maps. Site occupancies of O1 of metal-hydroxide layers were found to be close to 100% and fixed, while the occupancy of M site was fixed in accord with the chemical composition. The occupancy of C site has been fixed in accord with the charge balance. The refinement of site occupancies of interlayer oxygen atoms has shown an excess of electrons per formula unit

(*epfu*) that was treated as an excess of H<sub>2</sub>O molecules. The hydrogen atoms were localized from residual electron-density maps and refined using a riding model with U<sub>eq</sub> values restrained as 1.5 of donor O atom. The hydrogen atoms of the interlayer cannot be localized because of the high statistic disorder of the H<sub>2</sub>O molecules and carbonate groups.

**Table 6.** Selected bond distances (Å) for desautelsite including hydrogen bonding scheme.

Atom	Atom	Bond Distance	Atom	Atom	Bond Distance
M	O1	2.0719(13)	C	O2	1.593(6)
D–H	<i>d</i> (D–H)	<i>d</i> (H··· A)	<DHA	<i>d</i> (D··· A)	A
O1–H1	0.88(4)	2.11(5)	163.3(5)	2.96(4)	O2

## 4. Discussion

### 4.1. Crystal Structure

The crystal structure of desautelsite is built out of edge-shared octahedra  $M(\text{OH})_2$  ( $M = \text{Mg}_{0.77}\text{Mn}_{0.22}$ ) forming the octahedral sheet. The interlayer C atoms are located in the center of a prism built by H atoms of two neighboring octahedral sheets [35], while the interlayer O atoms of  $(\text{CO}_3)^{2-}$  group and  $(\text{H}_2\text{O})^0$  molecules are disordered around the prism edge (Figure 6). The interlayer C and O atom sites are low-occupied and statistically disordered, thus interlayer H atoms cannot be localized. The layers are stacked by rhombohedral periodicity producing the 3R polytype that is typical for hydrotalcite group minerals (Table 7). The powder X-ray diffraction pattern recorded from larger samples has also shown only the 3R polytype of desautelsite and the absence of any superstructure reflections. A similar situation with 3R polytype findings is also characteristic for Fe<sup>3+</sup>-analogues of desautelsite: pyroaurite and iowaite (Table 7).

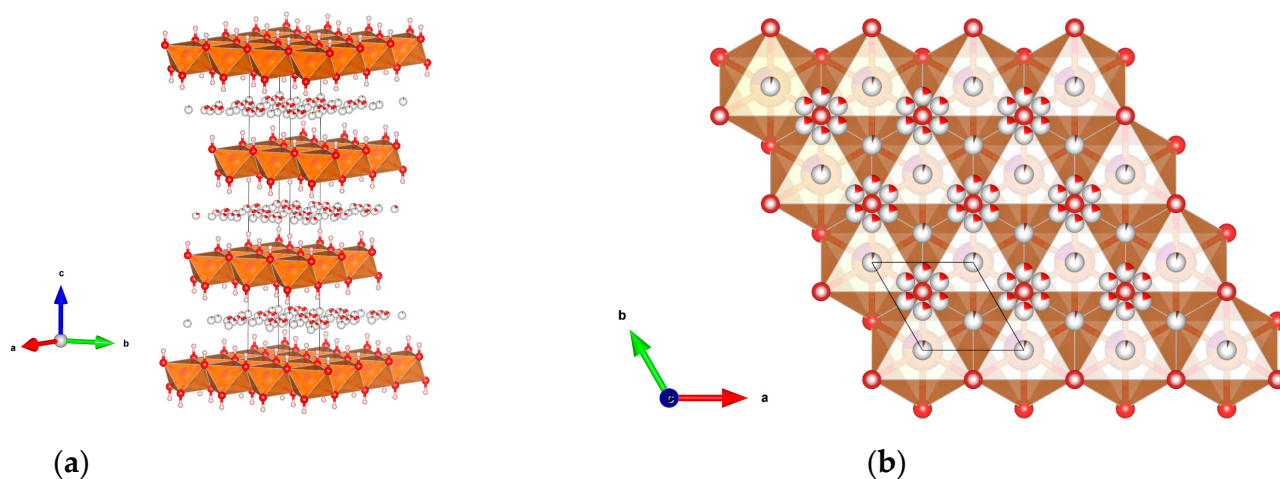


**Figure 6.** The crystal structure of desautelsite (a) and the projection of one octahedral sheet ( $z = 0$ ) and superimposed interlayer ( $z = 1/6$ ) (b). The unit-cell is outlined. Octahedra— $(\text{Mg}_{0.77}\text{Mn}_{0.22})(\text{OH})_2$ , O—red, H—white, C—brown. Sectors indicate site occupancy.

Table 7. Symmetry, polytype and unit-cell parameters of hydrotalcite group minerals.

Mineral	Empirical Chemical Formula	Space Group	Polytype	<i>a</i> , Å	<i>c</i> , Å	<i>V</i> , Å <sup>3</sup>	Comment <sup>1</sup>	Reference
Desautelsite	Mg <sub>6.20</sub> (Mn <sup>III</sup> <sub>1.78</sub> Al <sub>0.01</sub> Fe <sup>III</sup> <sub>0.01</sub> )(OH) <sub>16</sub> (CO <sub>3</sub> ) <sub>0.90</sub> ·5.35H <sub>2</sub> O	<i>R</i> -3 <i>m</i>	3 <i>R</i>	3.124	23.528	198.8	SC	This work, 29D
	Mg <sub>6.18</sub> Mn <sup>III</sup> <sub>1.82</sub> (OH) <sub>16</sub> (CO <sub>3</sub> ) <sub>1</sub> · <i>n</i> H <sub>2</sub> O	<i>R</i> -3 <i>m</i>	3 <i>R</i>	3.119	23.49	197.9	P	This work, 80137
	Mg <sub>6</sub> Mn <sup>III</sup> <sub>2</sub> (OH) <sub>16</sub> (CO <sub>3</sub> ) <sub>1</sub> ·4H <sub>2</sub> O	<i>R</i> 3 <i>m</i> or <i>R</i> -3 <i>m</i>	3 <i>R</i>	3.114	23.390	194.4	SC	[11]
Hydrotalcite	Mg <sub>5.88</sub> Al <sub>1.82</sub> Fe <sup>3+</sup> <sub>0.30</sub> (OH) <sub>16</sub> (CO <sub>3</sub> ) <sub>1.06</sub> ·4H <sub>2</sub> O	<i>R</i> -3 <i>m</i>	3 <i>R</i>	3.073	23.326	190.7	SC	[25]
	Mg <sub>5.87</sub> Al <sub>2.10</sub> Fe <sup>3+</sup> <sub>0.02</sub> (OH) <sub>16</sub> (CO <sub>3</sub> ) <sub>1.06</sub> ·4H <sub>2</sub> O	<i>P</i> 6 <sub>3</sub> / <i>mmc</i>	2 <i>H</i>	3.046	15.477	124.4		
Pyroaurite	Mg <sub>6.08</sub> Fe <sup>3+</sup> <sub>1.76</sub> Al <sub>0.17</sub> (OH) <sub>16</sub> (CO <sub>3</sub> ) <sub>1.00</sub> ·4H <sub>2</sub> O	<i>R</i> -3 <i>m</i>	3 <i>R</i>	3.126	23.520	199.0	SC	[31]
	Mg <sub>5.95</sub> Mn <sub>0.05</sub> Fe <sup>3+</sup> <sub>2.00</sub> (OH) <sub>16</sub> (CO <sub>3</sub> ) <sub>1.00</sub> ·4H <sub>2</sub> O	<i>R</i> -3 <i>m</i>	3 <i>R</i>	3.101	23.340	194.3	SC	
Iowaite	(Mg <sub>5.9</sub> Fe <sup>2+</sup> <sub>0.1</sub> )Fe <sup>3+</sup> <sub>2</sub> (OH) <sub>16</sub> [Cl <sub>1.4</sub> (OH) <sub>0.48</sub> (CO <sub>3</sub> ) <sub>0.06</sub> ]·4H <sub>2</sub> O	<i>R</i> -3 <i>m</i>	3 <i>R</i>	3.118	24.113	203.1	SC	[36]
	Mg <sub>6.11</sub> (Fe <sup>3+</sup> <sub>0.85</sub> Cr <sub>0.78</sub> Al <sub>0.26</sub> )(OH) <sub>16</sub> Cl <sub>1.82</sub> ·4H <sub>2</sub> O	<i>R</i> -3 <i>m</i>	3 <i>R</i>	3.110	24.120	202.0	P	[32]
		<i>P</i> 6 <sub>3</sub> / <i>mmc</i>	2 <i>H</i>	3.110	16.080	134.7	P	
Stichtite Fe <sup>3+</sup> -rich	Mg <sub>6.02</sub> Fe <sup>3+</sup> <sub>1.67</sub> Al <sub>0.31</sub> (OH) <sub>16.00</sub> Cl <sub>1.67</sub> (BO <sub>3</sub> ) <sub>0.11</sub> ·4H <sub>2</sub> O	<i>R</i> -3 <i>m</i>	3 <i>R</i>	3.108	23.885	199.8	SC	[37]
		<i>P</i> 6 <sub>3</sub> / <i>mmc</i>	2 <i>H</i>	3.100	15.700	130.9	P	[32]
Stichtite	n.g., possibly close to ideal Mg <sub>6</sub> Cr <sub>2</sub> (OH) <sub>16</sub> (CO <sub>3</sub> )·4H <sub>2</sub> O	<i>R</i> -3 <i>m</i>	3 <i>R</i>	3.096	23.507	195.1	P	[38]
		<i>P</i> 6 <sub>3</sub> / <i>mmc</i>	2 <i>H</i>	3.097	15.619	129.7	P	
		<i>P</i> 6 <sub>3</sub> / <i>mmc</i>	2 <i>H</i>	3.096	15.627	129.8	P	
Woodallite	Mg <sub>6.19</sub> (Cr <sub>1.21</sub> Fe <sub>0.51</sub> Al <sub>0.15</sub> )(OH) <sub>16</sub> [Cl <sub>1.62</sub> (CO <sub>3</sub> ) <sub>0.17</sub> (SO <sub>4</sub> ) <sub>0.01</sub> ]·4H <sub>2</sub> O	<i>R</i> -3 <i>m</i>	3 <i>R</i>	3.103	24.111	201.1	P	[39]
		n.g.	<i>R</i> -3 <i>m</i>	3 <i>R</i>	3.101	23.682	197.2	P
Kaznakhtite	(Ni <sub>5.54</sub> Mg <sub>0.47</sub> Zn <sub>0.02</sub> )(Co <sup>3+</sup> <sub>1.83</sub> Cr <sub>0.11</sub> Al <sub>0.03</sub> )(OH) <sub>15.84</sub> C <sub>1.00</sub> O <sub>2.99</sub> Cl <sub>0.16</sub> ·4H <sub>2</sub> O	<i>R</i> -3 <i>m</i>	3 <i>R</i>	3.052	23.180	186.9	P	[41]
Reevesite	(Ni <sub>5.837</sub> Mg <sub>0.106</sub> )(Fe <sup>3+</sup> <sub>1.804</sub> Co <sup>3+</sup> <sub>0.189</sub> )(OH) <sub>16</sub> (CO <sub>3</sub> ) <sub>0.92</sub> (SO <sub>4</sub> ) <sub>0.076</sub> · <i>n</i> H <sub>2</sub> O	n.g. <i>R</i> -3 <i>m</i> (?)	n.g. 3 <i>R</i>	3.085	23.355	192.5	P	[42]

Table 7. Cont.

Mineral	Empirical Chemical Formula	Space Group	Polytype	$a$ , Å	$c$ , Å	$V$ , Å <sup>3</sup>	Comment <sup>1</sup>	Reference
Takovite	n.g. <sup>2</sup> ?	$R\text{-}3m$	3R	3.029	22.599	179.6	SC	[40]
Droninoite	$(\text{Ni}_{2.16}\text{Fe}^{2+}_{0.75}\text{Fe}^{3+}_{0.97})(\text{OH})_{7.10}\text{Cl}_{1.62}\cdot 2.28\text{H}_2\text{O}$ <sup>3</sup>	$R\text{-}3m$	?	6.206 <sup>3</sup>	46.184	1540.4	P	[43]
Meixnerite	$\text{Mg}_6(\text{Al}_{1.95}\text{Fe}^{3+}_{0.05})(\text{OH})_{16}(\text{OH})_2\cdot 4\text{H}_2\text{O}$	$R\text{-}3m$	3R	3.046	22.930	184.2	P	[44]

<sup>1</sup> Unit-cell parameter determination using SC—single-crystal X-ray diffraction and P—powder X-ray diffraction. <sup>2</sup> The empirical chemical formula is not provided; the ideal chemical formula of takovite is  $\text{Ni}_6\text{Al}^{3+}_2(\text{OH})_{16}(\text{CO}_3)\cdot 4\text{H}_2\text{O}$ ; however, the experimentally determined occupancies indicate Ni:Al~2:1 rather than 3:1. <sup>3</sup>  $\text{Fe}_{\text{tot}}$  has been calculated [43] based on the condition that  $M^{\text{II}}:M^{\text{III}} = 3:1$ ; the  $a$  and  $c$  parameters are likely doubled since no superstructure reflections are reported leading to  $a = 3.103$  Å and  $c = 23.092$  Å in resemblance to other hydroxalcalite group minerals; and the polytype is likely classic 3R. Note: n.g.—not given.

Our data on the crystal structure of desautelsite completely agrees with those obtained previously [11] in terms of crystal structure topology. Thus, we confirm that the arrangement of  $Mg^{II}$  and  $Mn^{III}$  within an octahedral sheet should be realized in terms of short-range order. It is worth noting that the absence of  $M^{II}$  and  $M^{III}$  cation ordering agrees with all recent crystal structure studies of minerals from the hydrotalcite group constructing a hydrotalcite supergroup (Table 7). Therefore, it seems that the nature of the divalent and trivalent cations in this case does not affect the way they are located inside the layer, while the cation ratio  $M^{II}:M^{III}$  is decisive. At the same time, as noted in the Introduction section, cation ordering occurs in minerals belonging to the quintinite, cualstibite, wermlandite, fougèrite and hydrocalumite groups of the hydrotalcite supergroup having another stoichiometry and, in particular, a  $M^{II}:M^{III}$  cation ratio.

#### 4.2. Chemical Composition

The electron microprobe analysis allowed us to determine the empirical formula of the desautelsite under study as  $Mg_{6.20}(Mn^{III}_{1.78}Al_{0.01}Fe^{III}_{0.01})_{\Sigma 1.80}(OH)_{16}(CO_3)_{0.90} \cdot 5.35H_2O$ . When compared to the idealized chemical formula of desautelsite,  $Mg_6Mn^{III}_2(OH)_{16}(CO_3)_{1.0} \cdot 4H_2O$ , the samples under study have a higher  $M^{II}:M^{III}$  ratio of 3.4:1 (Table 1). The chemical composition study suggested a higher content of interlayer  $H_2O$  molecules: 5 *apfu* instead of 4 *apfu* based on measured totals and their consistency. The crystal structure refinement has also indicated a higher content of interlayer  $H_2O$  molecules by the occupancy of the interlayer O2 site (Table 5). The higher content of interlayer ( $H_2O$ ) molecules may be due to a higher ratio of  $M^{II}:M^{III}$  when compared to the ideal stoichiometry. The Raman spectroscopy of desautelsite samples has shown the presence of only the  $(CO_3)^{2-}$  anion in the interlayer (Table 2).

#### 4.3. Octahedral Sheet: Chemistry, Cation Radii and Octahedra Distortion

From the crystal structure refinement, we can conclude that for hydrotalcite group minerals,  $M^{II}$  and  $M^{III}$  cations are disordered (in terms of long-range structure) despite the nature of  $M^{II}$  (Mg, Ni) and  $M^{III}$  (Al, Fe, Mn, Cr, Co) cations. However, the nature of cations should affect geometrical parameters of the crystal structure, such as  $M-O$  bond length, polyhedral size and, thus, interplanar  $a$  unit cell parameter (Figure 7). In order to estimate this quantitatively, we have calculated the averaged crystal radius that is the type of effective ionic radius [26] as

$$\text{averaged crystal radius} = \frac{\sum \text{apfu of cation} \times \text{cation radius}}{\sum \text{apfu of cation}}$$

The crystal radii of cations are taken from [26], the cation *apfu* (contents) are taken from Table 7. For example, for the desautelsite described by [11] the averaged cation radius of metals constructing octahedral sheet is calculated as  $\sum (6 \times 0.86 + 2 \times 0.785) \div 8 = 0.8413$  (where 6-*apfu* for Mg, 2-*apfu* for  $Mn^{III}$ , 0.86-crystal radius of Mg, 0.785-crystal radius of  $Mn^{III}$ , 8-*apfu* for cation sum). This averaged cation radius can be correlated to the in-plane  $a$  parameter of the unit cell providing predictive power: the  $a$  unit cell parameter can be calculated from the chemical composition and compared to the correlation and *vice versa* that allows, for instance, control of cation intercalation in synthetic LDHs. The experimentally obtained correlation,  $y = 1.987x + 1.4455$  (where  $y$ — $a$  unit cell parameter and  $x$ —averaged cation radius) (Figure 7) is based on 11 well-characterized natural samples (see references in Table 7 and Figure 7) and shows good agreement with  $R^2 = 0.91$  ( $R^2$  is the goodness of fit for linear correlation). The strongest deviation from the approximated line is observed for pyroaurite, possibly because the precise determination of the  $M^{II}:M^{III}$  ratio is problematic since some minor Fe may be in divalent form. However, this deviation does not extend to iowaite which is identical to pyroaurite in cation contents and their ratio, i.e.,  $Mg:Fe^{III} = 3:1$ . The deviation from approximation is also observed for reevesite (Figure 7), which is because the mineral has slightly variable cation content, and the unit-cell parameters are calculated for the general sample and not for precise

chemical variety. Desautelsite agrees well with the approximation being the end-member with the highest  $a$  unit cell parameter, due to the presence of the large trivalent cation ( $\text{Mn}^{\text{III}}$ ) in its chemical composition that is comparable to  $\text{Fe}^{\text{III}}$  that, in turn, is the dominant trivalent cation in pyroaurite and iowaite (Figure 7). In general, natural LDHs can be model systems for constructing such correlations between the geometric parameters of the crystal structure and the chemical composition of the mineral, and can easily be approximated to synthetics, which require simple and high-quality control over the chemical composition. Obviously, the weak crystal-chemical characteristics of many minerals of the hydrotalcite supergroup, including the hydrotalcite group itself (Table 7), still remain a problematic side.

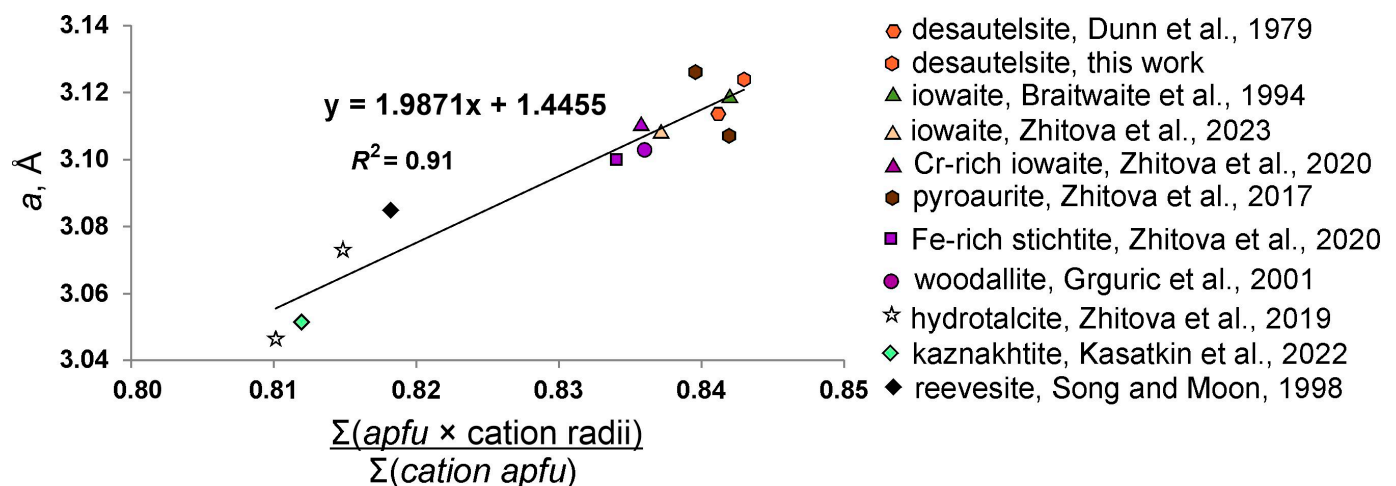


**Figure 7.** The correlation between averaged cation radii of metals constructing the octahedral sheet and the in-plane  $a$  unit cell parameter for hydrotalcite group minerals using data reported therein and in [11,25,31,32,36,37,39,41,42]. Note: the data without chemical composition are not included; droninoite [43] is omitted since  $\text{Fe}^{2+}/\text{Fe}^{3+}$  is not known.

## 5. Conclusions

The crystal structure refinement has indicated that desautelsite crystallizes as a classic  $3R$  polytype with  $\text{Mg}^{\text{II}}$  and  $\text{Mn}^{\text{III}}$  being disordered (in terms of long-range order) and occupying one  $M$  site,  $\text{Mg}_{0.77}\text{Mn}_{0.23}$ . The arrangement of Mg and Mn within an octahedral sheet should be short-range ordered in nature. The important outcome is that for hydrotalcite group minerals having  $M^{\text{II}}:M^{\text{III}} = 3:1$ , the cation organization within metal-hydroxide sheets seems to be determined by the cation ratio rather than specific (or the nature of) di- and trivalent cations. The interlayer species are located in-between two octahedral sheets: C atoms occupy the center of the trigonal prism, while O atoms of  $(\text{H}_2\text{O})^0$  and  $(\text{CO}_3)^{2-}$  are disordered around the prism edge. The topology of desautelsite corresponds to the classic  $3R$  polytype (with carbonate interlayer) which also extends at least to hydrotalcite group minerals with recently refined structures such as hydrotalcite, pyroaurite, stichtite and kaznakhtite.

The available literature and our data make it possible to construct a correlation between the cation size and the unit cell parameter  $a$ . The latter is quite easy to calculate from routine X-ray powder diffraction data. Using the provided correlation [between the averaged cation effective ionic radius (crystal radius in accord with Shannon) ( $x$ ) and  $a$  unit cell parameter ( $y$ ),  $y = 1.9871x + 1.4455$ ], the  $a$  unit cell parameter can be related to the chemical composition of the LDH compound. In practice, this would be useful for checking isomorphic substitution (especially in the case of cations of different sizes) or for monitoring the compliance of the  $M^{\text{II}}:M^{\text{III}}$  ratio with the assumed value. In this case, it is natural LDHs that can serve as model systems for constructing such correlations since they form crystals and, due to this, it is easier to characterize them from the structural and chemical point of view.

**Supplementary Materials:** The following supporting information can be downloaded at: <https://www.mdpi.com/article/10.3390/sym15051029/s1>, Table S1: powder X-ray diffraction data for desautelsite sample 80137 including reflections of lizardite and dashkovaite and Table S2: anisotropic displacement parameters ( $\text{\AA}^2$ ) for desautelsite.

**Author Contributions:** Conceptualization, E.S.Z.; methodology, E.S.Z., A.V.K. and V.N.B.; software, E.S.Z., R.M.S., A.A.Z. and V.N.B.; validation, E.S.Z., R.M.S., A.V.K., A.A.Z., V.N.B., A.N.K. and D.I.B.; formal analysis, E.S.Z., R.M.S., A.V.K., V.N.B. and A.N.K.; investigation, E.S.Z., R.M.S., A.A.Z., V.N.B. and A.V.K.; resources, A.V.K. and D.I.B.; data curation, A.A.Z., V.N.B., A.V.K. and D.I.B.; writing—original draft preparation, E.S.Z., R.M.S., V.N.B. and A.V.K.; writing—review and editing, E.S.Z., R.M.S., A.A.Z., V.N.B., A.V.K., A.N.K. and D.I.B.; visualization, E.S.Z., R.M.S., V.N.B. and A.N.K.; supervision, E.S.Z., A.A.Z. and A.V.K.; project administration, E.S.Z.; funding acquisition, E.S.Z. All authors have read and agreed to the published version of the manuscript.

**Funding:** This research was funded by the Russian Science Foundation, grant number 22-77-10036.

**Data Availability Statement:** The crystallographic information file (cif) has been deposited via the joint Cambridge Crystal Data Centre CCDC/FIZ Karlsruhe deposition service; the deposition number is 2251692.

**Acknowledgments:** The technical support of St. Petersburg State University Resource Centers “XRD” and “Geomodel” is gratefully acknowledged. We thank Natalia Vlasenko for the preliminary electron-microprobe data.

**Conflicts of Interest:** The authors declare no conflict of interest.

## References

1. Liu, P.; Wang, H.; Feng, Z.; Ying, P.; Li, C. Direct immobilization of self-assembled polyoxometalate catalyst in layered double hydroxide for heterogeneous epoxidation of olefins. *J. Catal.* **2008**, *256*, 345–348. [[CrossRef](#)]
2. Yu, J.; Fan, G.; Yang, Y.; Li, F. Multi-level three-dimensional Mg–Al layered double hydroxide hierarchical microstructures with enhanced basic catalytic property. *J. Colloid Interf. Sci.* **2014**, *432*, 1–9. [[CrossRef](#)]
3. Fan, G.; Li, F.; Evans, D.G.; Duan, X. Catalytic applications of layered double hydroxides: Recent advances and perspectives. *Chem. Soc. Rev.* **2014**, *43*, 7040–7066. [[CrossRef](#)] [[PubMed](#)]
4. Béléké, A.B.; Mizuhata, M. Electrochemical properties of nickel–aluminum layered double hydroxide/carbon composite fabricated by liquid phase deposition. *J. Power Sources* **2010**, *195*, 7669–7676. [[CrossRef](#)]
5. Choy, J.H.; Kwak, S.Y.; Park, J.S.; Jeong, Y.J. Cellular uptake behavior of [ $\gamma$ -32P] labeled ATP–LDH nanohybrids. *J. Mater. Chem.* **2001**, *11*, 1671–1674. [[CrossRef](#)]
6. Nalawade, P.; Aware, B.; Kadam, V.J.; Hirekar, R.S. Layered double hydroxides: A review. *J. Sci. Ind. Res. India.* **2009**, *68*, 267–272.
7. Conterosito, E.; Croce, G.; Palin, L.; Pagano, C.; Perioli, L.; Viterbo, D.; Boccaleri, E.; Paul, G.; Milanese, M. Structural characterization and thermal and chemical stability of bioactive molecule–hydrotalcite (LDH) nanocomposites. *Phys. Chem. Chem. Phys.* **2013**, *15*, 13418–13433. [[CrossRef](#)]
8. Duan, X.; Evans, D.G. *Layered Double Hydroxides*; Springer: Berlin/Heidelberg, Germany, 2006. [[CrossRef](#)]
9. Tronto, J.; Crepaldi, E.L.; Pavan, P.C.; Cipriano De Paula, C.; Valim, J.B. Organic anions of pharmaceutical interest intercalated in magnesium aluminum LDHs by two different methods. *Mol. Cryst. Liq. Cryst.* **2001**, *356*, 227–237. [[CrossRef](#)]
10. Mills, S.J.; Christy, A.G.; Génin, J.M.; Kameda, T.; Colombo, F. Nomenclature of the hydrotalcite supergroup: Natural layered double hydroxides. *Mineral. Mag.* **2012**, *76*, 1289–1336. [[CrossRef](#)]
11. Dunn, P.J.; Peacor, D.R.; Palmer, T.D. Desautelsite, a new mineral of the pyroaurite group. *Am. Mineral.* **1979**, *64*, 127–130.
12. Matsubara, S.; Kato, A.; Nagashima, K. Desautelsite from Konomori, Kochi City, Japan. *Bull. Natl. Sci. Mus.* **1984**, *10*, 81–86.
13. Hofmeister, W.; Platen, H.V. Crystal chemistry and atomic order in brucite-related double-layer structures. *Crystallogr. Rev.* **1992**, *3*, 3–26. [[CrossRef](#)]
14. Richardson, I.G. Classification of possible ordered distributions of trivalent cations in layered double hydroxides and an explanation for the observed variation in the lower solid-solution limit. *Acta Crystallogr. B* **2013**, *69*, 629–633. [[CrossRef](#)] [[PubMed](#)]
15. Bonaccorsi, E.; Merlino, S.; Orlandi, P. Zincalstibite, a new mineral, and cualstibite: Crystal chemical and structural relationships. *Am. Mineral.* **2007**, *92*, 198–203. [[CrossRef](#)]
16. Mills, S.J.; Kampf, A.R.; Housley, R.M.; Favreau, G.; Pasero, M.; Biagioni, C.; Merlino, S.; Berbain, C.; Orlandi, P. Omsite,  $(\text{Ni,Cu})_2\text{Fe}^{3+}(\text{OH})_6[\text{Sb}(\text{OH})_6]$ , a new member of the cualstibite group from Oms, France. *Mineral. Mag.* **2012**, *76*, 1347–1354. [[CrossRef](#)]
17. Mills, S.J.; Christy, A.G.; Kampf, A.R.; Housley, R.M.; Favreau, G.; Boulliard, J.-C.; Bourgoin, V. Zincalstibite-9R: The first nine-layer polytype with the layered double hydroxide structure-type. *Mineral. Mag.* **2012**, *76*, 1337–1345. [[CrossRef](#)]
18. Kolitsch, U.; Giester, G.; Pippinger, T. The crystal structure of cualstibite-1M (formerly cyanophyllite), its revised chemical formula and its relation to cualstibite-1T. *Mineral. Petrol.* **2013**, *107*, 171–178. [[CrossRef](#)]

19. Zhitova, E.S.; Krivovichev, S.V.; Yakovenchuk, V.N.; Ivanyuk, G.Y.; Pakhomovsky, Y.A.; Mikhailova, J.A. Crystal chemistry of natural layered double hydroxides: 4. Crystal structures and evolution of structural complexity of quintinite polytypes from the Kovdor alkaline-ultrabasic massif, Kola peninsula, Russia. *Mineral. Mag.* **2018**, *82*, 329–346. [[CrossRef](#)]
20. Zhitova, E.S.; Krivovichev, S.V.; Pekov, I.V.; Yapaskurt, V.O. Crystal chemistry of chlormagaluminite,  $Mg_4Al_2(OH)_{12}Cl_2(H_2O)_2$ , a natural layered double hydroxide. *Minerals* **2019**, *9*, 221. [[CrossRef](#)]
21. Rius, J.; Allmann, R. The superstructure of the double layer mineral wermlandite  $[Mg_7(Al_{0.57}, Fe^{3+}_{0.43})_2(OH)_{18}]^{2+}[(Ca_{0.6}, Mg_{0.4})(SO_4)_2(H_2O)_{12}]^{2-}$ . *Z. Fur Krist.* **1984**, *168*, 133–144. [[CrossRef](#)]
22. Cooper, M.A.; Hawthorne, F.C. The crystal structure of shigaite,  $[AlMn_2^{2+}(OH)_6]_3(SO_4)_2Na(H_2O)_6(H_2O)_6$ , a hydrotalcite group mineral. *Can. Mineral.* **1996**, *34*, 91–97.
23. Huminicki, D.M.C.; Hawthorne, F.C. The crystal structure of nikischerite,  $NaFe_6^{2+}Al_3(SO_4)_2(OH)_{18}(H_2O)_{12}$ , a mineral of the shigaite group. *Can. Mineral.* **2003**, *41*, 79–82. [[CrossRef](#)]
24. Zhitova, E.S.; Chukanov, N.V.; Jonsson, E.; Pekov, I.V.; Belakovskiy, D.I.; Vigasina, M.F.; Zubkova, N.V.; Van, K.V.; Britvin, S.N. Erssonite,  $CaMg_7Fe^{3+}_2(OH)_{18}(SO_4)_2 \cdot 12H_2O$ , a new hydrotalcite-super group mineral from Långban, Sweden. *Mineral. Mag.* **2021**, *85*, 817–826. [[CrossRef](#)]
25. Zhitova, E.S.; Krivovichev, S.V.; Pekov, I.; Greenwell, H.C. Crystal chemistry of natural layered double hydroxides. 5. Single-crystal structure refinement of hydrotalcite,  $[Mg_6Al_2(OH)_{16}](CO_3)(H_2O)_4$ . *Mineral. Mag.* **2019**, *83*, 269–280. [[CrossRef](#)]
26. Shannon, R.D. Revised effective ionic radii and systematic studies of interatomic distances in halides and chalcogenides. *Acta Crystallogr. A* **1976**, *32*, 751–767. [[CrossRef](#)]
27. Cisneros, S.L.; Witkowski, R.E.; Oswald, D.L. Artinite from San Benito County, California. *Mineral. Rec.* **1977**, *8*, 457–460.
28. Warr, L.N. IMA-CNMNC approved mineral symbols. *Mineral. Mag.* **2021**, *85*, 291–320. [[CrossRef](#)]
29. *CrysAlisPro Software System*, version 1.171.38.46; Rigaku Oxford Diffraction: Oxford, UK, 2015.
30. Frost, R.L.; Erickson, K.L. Raman spectroscopic study of the hydrotalcite desautelsite  $Mg_6Mn_2CO_3(OH)_{16} \cdot 4H_2O$ . *Spectrochim. Acta A Mol. Biomol. Spectrosc.* **2005**, *61*, 2697–2701. [[CrossRef](#)]
31. Zhitova, E.S.; Ivanyuk, G.Y.; Krivovichev, S.V.; Yakovenchuk, V.N.; Pakhomovsky, Y.A.; Mikhailova, Y.A. Crystal chemistry of pyroaurite from the Kovdor pluton, Kola peninsula, Russia, and the Långban Fe–Mn deposit, Värmland, Sweden. *Geol. Ore Depos.* **2017**, *59*, 652–661. [[CrossRef](#)]
32. Zhitova, E.S.; Pekov, I.V.; Chukanov, N.V.; Yapaskurt, V.O.; Bocharov, V.N. Minerals of the system stichtite–pyroaurite–iowaite–woodallite from serpentinites of the Terehta Ridge (Gorny Altai, Russia). *Russ. Geol. Geophys.* **2020**, *61*, 36–46. [[CrossRef](#)]
33. Mora, M.; Jiménez-Sanchidrián, C.; Ruiz, J.R. Raman spectroscopy study of layered-double hydroxides containing magnesium and trivalent metals. *Mater. Lett.* **2014**, *120*, 193–195. [[CrossRef](#)]
34. Britvin, S.N.; Dolivo-Dobrovolsky, D.V.; Krzhizhanovskaya, M.G. Software for processing of X-ray powder diffraction data obtained from the curved image plate detector of Rigaku RAXIS Rapid II diffractometer. *Zapiski RMO* **2017**, *146*, 104–107. (In Russian)
35. Bookin, A.S.; Drits, V.A. Polytype diversity of the hydrotalcite-like minerals I. Possible polytypes and their diffraction features. *Clays Clay Miner.* **1993**, *41*, 551–557. [[CrossRef](#)]
36. Braithwaite, R.S.W.; Dunn, P.J.; Pritchard, R.G.; Paar, W.H. Iowaite, a re-investigation. *Mineral. Mag.* **1994**, *58*, 79–85. [[CrossRef](#)]
37. Zhitova, E.S.; Chukanov, N.V.; Pekov, I.V.; Zolotarev, A.A.; Shilovskikh, V.V.; Bocharov, V.N. Crystal chemistry of iowaite,  $Mg_6Fe^{+3}_2(OH)_{16}Cl_2 \times 4H_2O$ , a natural layered double hydroxide. *Appl. Clay Sci.* **2023**.
38. Mills, S.J.; Whitfield, P.S.; Wilson, S.A.; Woodhouse, J.N.; Dipple, G.M.; Raudsepp, M.; Francis, C.A. The crystal structure of stichtite, re-examination of barbertonite, and the nature of polytypism in MgCr hydrotalcites. *Am. Mineral.* **2011**, *96*, 179–187. [[CrossRef](#)]
39. Grguric, B.A.; Madsen, I.C.; Pring, A. Woodallite, a new chromium analogue of iowaite from the Mount Keith nickel deposit, Western Australia. *Mineral. Mag.* **2001**, *65*, 427–435. [[CrossRef](#)]
40. Mills, S.J.; Whitfield, P.S.; Kampf, A.R.; Wilson, S.A.; Dipple, G.M.; Raudsepp, M.; Favreau, G. Contribution to the crystallography of hydrotalcites: The crystal structures of woodallite and takovite. *J. Geosci.* **2012**, *57*, 273–279. [[CrossRef](#)]
41. Kasatkin, A.V.; Britvin, S.N.; Krzhizhanovskaya, M.G.; Chukanov, N.V.; Škoda, R.; Göttlicher, J.; Belakovskiy, D.I.; Pekov, I.V.; Levitskiy, V.V. Kaznakhtite,  $Ni_6Co^{3+}_2(CO_3)(OH)_{16} \cdot 4H_2O$ , a new natural layered double hydroxide, the member of the hydrotalcite supergroup. *Mineral. Mag.* **2022**, *86*, 841–848. [[CrossRef](#)]
42. Song, Y.; Moon, H.S. Additional data on reevesite and its Co-analogue, as a new member of the hydrotalcite group. *Clay Mineral.* **1998**, *33*, 285–296. [[CrossRef](#)]
43. Chukanov, N.V.; Pekov, I.V.; Levitskaya, L.A.; Zadov, A.E. Droninoite,  $Ni_3Fe^{3+}Cl(OH)_8 \cdot 2H_2O$ , a new hydrotalcite-group mineral species from the weathered Dronino meteorite. *Geol. Ore Depos.* **2009**, *51*, 767–773. [[CrossRef](#)]
44. Koritnig, S.; Süsse, P. Meixnerit,  $Mg_6Al_2(OH)_{18} \cdot 4H_2O$ , ein neues Magnesium-Aluminium-Hydroxid-Mineral. *Tschermaks Mineral. Petrogr. Mitt.* **1975**, *22*, 79–87. [[CrossRef](#)]

**Disclaimer/Publisher’s Note:** The statements, opinions and data contained in all publications are solely those of the individual author(s) and contributor(s) and not of MDPI and/or the editor(s). MDPI and/or the editor(s) disclaim responsibility for any injury to people or property resulting from any ideas, methods, instructions or products referred to in the content.